scientific reports

Check for updates

OPEN

Efficacy of Naringenin against aging and degeneration of nucleus pulposus cells through IGFBP3 inhibition

Xiaokai Tang[1,2,3,6], Junlong Zhong[2,6], Hao Luo[2,3,6], Faxin Zhou[2,3], Lixia Wang[2,3], Sijian Lin[4], Jiachao Xiong[2], Hao Lv[2,3], Zhenhai Zhou[2], Honggui Yu[2✉] & Kai Cao[3,5✉]

Naringenin (NAR), a natural flavonoid, exerts anti-inflammatory and antioxidant pharmacology. However, the pharmacological mechanisms through which NAR prevents and treats intervertebral disc degeneration (IDD) remain unclear. We utilized bioinformatics, machine learning, and network pharmacology to identify shared targets among NAR, senescence, and IDD. Subsequently, molecular docking was conducted to evaluate NAR's binding affinity to common target. Additionally, we used IL-1β to induce senescence and degeneration in nucleus pulposus cells (NPCs) and conducted a series of cellular assays, including immunoblotting, immunofluorescence, β-galactosidase staining, cell proliferation, cell cycle analysis, and measurement of reactive oxygen species levels, to investigate NAR's impact on IL-1β-induced senescence and degeneration of NPCs. Our study revealed that Insulin-like growth factor binding protein 3 (IGFBP3) was the only common target. IGFBP3 exhibited significant differences between the IDD and healthy groups and proved to be an effective diagnostic marker for IDD. Molecular docking confirmed the binding between NAR and IGFBP3. In vitro experiments, we observed that Igfbp3 expression increased in the senescence and degeneration groups. Igfbp3 knockdown and NAR attenuated IL-1β-induced senescence and degenerative phenotypes in NPCs. In contrast, the effect of NAR was attenuated by recombinant IGFBP3 protein. In conclusion, our findings suggest that NAR plays a preventive and therapeutic role in IDD, likely achieved through the inhibition of Igfbp3 expression.

Abbreviations

NAR	Naringenin
IDD	Intervertebral disc degeneration
NP	Nucleus pulposus
NPCs	Nucleus pulposus cells
IGFBP3	Insulin-like growth factor binding protein 3
IVD	Intervertebral disc
SASP	Senescence-associated secretory phenotype
ECM	Extracellular matrix
ARGs	Aging related genes
DEGs	Differentially expressed genes
GO	Gene ontology
KEGG	Kyoto encyclopedia of genes and genomes

[1]Department of Orthopedics, People's Hospital of Deyang City, Deyang, China. [2]Orthopedic Hospital, The First Affiliated Hospital, Jiangxi Medical College, Nanchang University, #1519 Dongyue Avenue, Nanchang 330209, Jiangxi, China. [3]The Key Laboratory of Spine and Spinal Cord Disease of Jiangxi Province, Nanchang 330006, China. [4]Department of Rehabilitation Medicine, The Second Affiliated Hospital, Jiangxi Medical College, Nanchang University, Nanchang, Jiangxi, China. [5]Department of Orthopedics, Affiliated Rehabilitation Hospital of Nanchang University, Nanchang 330002, China. [6]Xiaokai Tang, Junlong Zhong and Hao Luo contributed equally to this work. ✉email: xiatiantian0702@126.com; kaichaw@126.com; Ndyfy09561@ncu.edu.cn

LASSO	Least absolute shrinkage and selection operator
SVM	Support vector machine
ROC	Receiver operating characteristic
AUC	Area under the curve
SA-β-Gal	Senescence-associated β-galactosidase
ROS	Reactive oxygen species

Intervertebral disc (IVD) degeneration (IDD) represents a pervasive age-associated health issue, often identified as the principal causative factor of lumbar back pain[1,2]. Research indicates that >70% of the world's population will encounter lumbar back pain at some juncture in their lives[3,4], leading to significant global economic repercussions[5–7]. The IVD primarily consists of the fibrous annulus, nucleus pulposus (NP), and cartilaginous endplate, linking adjacent vertebrae[8,9]. Any compromise to these components can trigger IDD. The pathogenesis of IDD is profoundly complex, involving many biological processes, such as cellular senescence, inflammatory responses, oxidative stress, and cellular apoptosis[10,11]. Over the past three decades, extensive research has aimed at ameliorating IDD[12–14]. Unfortunately, current therapeutic approaches are inadequate to treat IVD or inhibit degeneration in IDD[15]. Therefore, effective strategies are urgently needed for preventing and treating IDD.

Cell senescence refers to the state where the cell cycle is continuously arrested, preventing cells from proliferating normally[16]. Another prominent feature of senescent cells is the senescence-associated secretory phenotype (SASP)[17], which stimulates adjacent cells to accelerate their own aging through autocrine and paracrine pathways[18]. Senescence is indispensable for IDD onset and progression. Senescent cells accumulated within the IVD drive IDD progression[19,20]. Despite constituting a relatively small proportion within the IVD, NP cells (NPCs) play an irreplaceable role in maintaining the structural and functional integrity of the IVD[21]. Studies have shown that during the occurrence and development of IDD, senescent NPCs gradually increase in number, severely affecting the synthesis of the extracellular matrix (ECM) within IVD, thereby accelerating IVD degeneration[18]. During IVD degeneration, IL-1β levels significantly increase in degenerated IVD tissues. IL-1β is involved in various pathological processes, including ECM degradation, oxidative stress, and cell senescence[22]. Therefore, inhibiting IL-1β-induced oxidative stress and senescence is a potential strategy to prevent IDD progression.

Naringenin (NAR) is natural flavonoid, predominantly found in citrus fruits[23], especially grapefruit[24]. NAR has anti-inflammatory[25], antioxidant[23], and anti-fibrotic effects[26], exerting potent protective roles in the management of heart disease, liver disorders, metabolic irregularities, etc[27,28]. Studies have shown that NAR offers protection against iron overload-induced osteoarthritis by inhibiting oxidative stress[29]. NAR improves vascular health and mitigates atherosclerosis by activating SIRT1[30]. In a rodent colitis model, NAR provides protective effects by reducing the production of inflammatory cytokines, such as tumor necrosis factor-α, IL-1, and IL-6[31]. However, studies on the roles of NAR in antiaging and antidegeneration in NPCs are lacking.

Network pharmacology is an interdisciplinary field that integrates bioinformatics, computational biology, and pharmaceutical research. It discerns latent pharmaceutical targets, elucidating the mechanisms of drug action and facilitating the development of innovative treatments for specific medical conditions[32]. Bioinformatics, an interdisciplinary field, uses methodologies and techniques from biology, computer science, and mathematics to collect, store, analyze, and interpret biological data[33]. Therefore, combining network pharmacology with bioinformatics in traditional Chinese medicine research may be effective for identifying therapeutic targets in IDD. This study integrated network pharmacology and bioinformatics to reveal the potential pharmacological impact of NAR in delaying aging and degeneration in NPCs by inhibiting insulin-like growth factor binding protein 3 (Igfbp3) expression. Additionally, the mechanism was confirmed through using an IL-1β-induced model of aging and degeneration in NPCs.

Materials and methods
Data collection and preprocessing
A search was performed in the GEO database using the keyword "intervertebral disc degeneration" under the specified conditions of "Series" and "*Homo sapiens*." The GSE56081, GSE70362, and GSE23130 datasets were chosen for analysis. GSE56081 comprised 5 normal and 5 degenerated samples; GSE70362 included 8 normal and 10 degenerated samples; and GSE23130 contained 6 normal and 8 degenerated samples. To merge the GSE56081 and GSE70362 datasets into a single dataset, normalization and batch effect removal techniques were applied using the "limma" and "sva" packages in R language. The merged dataset served as the training group, whereas the GSE23130 dataset served as the test group.

A search was conducted in the Traditional Chinese Medicine Systems Pharmacology Database and Analysis Platform (TCMSP; https://tcmspw.com)[34], DrugBank database (https://go.drugbank.com), Search Tool for Interactions of Chemicals database (STITCH; https://stitch.embl.de), and SwissTargetPrediction database (http://www.swisstargetprediction.ch)[35] to retrieve targets associated with "NAR." The relevant targets were transformed into their corresponding gene names through the UniProt database (https://www.uniprot.org/). Human aging related genes (ARGs) were obtained from GenAge: The Aging Gene Database (https://www.genomics.senescence.info/genes/index.html)[36]. All the study was performed in accordance with relevant guidelines and regulation.

Differential analysis and enrichment analysis
Differential analysis was performed using the "limma" package in the R programming language to identify differentially expressed genes (DEGs) in the training and test group datasets. The DEGs were visualized with volcano plots and heatmaps utilizing "pheatmap," "dplyr," "ggplot2," and "ggrepel" packages. Functional enrichment analysis using gene ontology (GO) of the DEGs was performed using "colorspace," "stringi,"

"ggplot2," and "GOplot" in R. We performed Kyoto Encyclopedia of Genes and Genomes (KEGG) pathway enrichment analysis on the DEGs using "clusterProfiler," "org.Hs.eg.db," and "enrichplot" packages and obtained images from KEGG[37–39].

Screening for disease diagnostic marker genes

Least absolute shrinkage and selection operator (LASSO) is a statistical technique used for linear regression and feature selection. It combines the merits of ridge regression and stepwise regression to shrink model parameters and select variables by restricting the coefficients[40]. LASSO possesses the advantage of automatically selecting the most pertinent features when identifying disease signature genes, reducing model complexity and enhancing interpretability. Support vector machine (SVM) is a supervised learning algorithm extensively used for classification and regression, exerting significant influence in machine learning. SVM operates on the principle of identifying an optimal hyperplane that maximally separates disease samples from normal samples. SVM can handle high-dimensional data, exhibit superior generalization ability, and provide deeper insights into disease characteristics, demonstrating adaptability to nonlinear problems[41]. In this study, LASSO, in combination with SVM, was used to screen DEGs for IDD-associated disease signature genes, facilitating subsequent analysis.

Screening and validation of core genes

In this study, important genes extracted from the analysis were identified as core genes through the intersecting analysis of ARGs, NAR-related targets, and diagnostic markers identified through LASSO regression and SVM techniques. Subsequently, variance in core gene expression was authenticated in training and test groups. The precision of using the core gene expression to forecast IDD status was evaluated through receiver operating characteristic (ROC) curves. Diagnostic efficacy was satisfactory when area under the curve (AUC) was > 0.7.

Molecular docking

The crystal structure of IGFBP3 was retrieved from the RCSB PDB database and processed using Schrödinger software, involving a multistep approach encompassing ligand state regeneration, optimization of H-bond assignments, energy minimization, and solvent removal. Subsequently, NAR's 2D sdf structure was processed and expanded to 3D chiral conformations using Schrödinger's LigPrep module. The SiteMap module identified optimal binding sites, and the receptor grid generation module configured an enclosing box for precise site mapping. Active sites within IGFBP3 were determined based on this information. Finally, molecular docking was performed between processed NAR and IGFBP3's active site, followed by MM-GBSA calculations to approximate binding free energy. Lower MM-GBSA dG bind values indicated greater ligand–protein binding stability.

Cell culture

Anesthetizing 4-week-old C57 mice (purchased from Changsha Tianqin Biotechnology Co.) with sodium pentobarbital (30 mg/kg), followed by euthanizing them using the cervical vertebra dislocating method. The lumbar and caudal vertebrae were collected, surrounding soft tissues were removed, and gelatinous NP tissues were extracted from the IVDs, then finely minced under aseptic conditions into pieces measuring 1 mm³, enzymatically digested using 0.25% EDTA-free trypsin (Solarbio, Beijing, China) at 37 °C for 30 min, and centrifuged to remove the supernatant. NP tissues were further digested with collagenase II (Solarbio, Beijing, China) at a concentration of 2 mg/mL for 6 h at 37 °C on a shaker. NPCs were cultured in Dulbecco's modified Eagle's medium supplemented with 15% fetal bovine serum (TransGen Biotech, Beijing, China) and 1% penicillin–streptomycin (Beyotime Biotechnology, Shanghai, China) at 37 °C with 5% CO_2. Once the cell density reached 90%, the cells were passaged, and only the first 3–5 generations were utilized for subsequent experiments. The animal studies involved in this study were approved by the Ethics Committee of the First Affiliated Hospital of Nanchang University. The ethics number is CDYFY-IACUC-202308QR034. All animal studies were performed in accordance with ARRIVE guidelines, and all methods were performed in accordance with the relevant guidelines and regulations[42].

Cell treatment and transfection

For the in vitro modeling of cellular senescence and degeneration, NPCs were exposed to 0, 10, and 20 ng/mL IL-1β (PeproTech, USA) for 48 h. To assess NAR's role in antiaging and antidegeneration, NPCs were treated with NAR (Selleck, USA) (0, 25, and 50 μM) or recombinant IGFBP3 (PeproTech, USA) (50 ng/mL) for 48 h.

To interfere with the expression of *Igfbp3*, we procured *Igfbp3*-targeting siRNAs (si-1 and si-2) and a non-targeting siRNA (si-NC) (GenePharma, China). NPCs were transfected with targeted or non-targeted siRNA duplexes using Lipofectamine 3000 siRNA Transfection Reagent (Thermo Fisher, USA). Cell harvesting for subsequent experiments occurred 48 h after transfection. siRNA sequences used in this study are detailed in Table 1.

CCK-8

In total, 5×10^3 primary mouse neural progenitor cells were seeded in 96-well plates and exposed to 0, 10, 20, 50, and 100 μg/mL of NAR for 24 and 48 h. Cells in each well were incubated with 10 μL of CCK-8 assay reagent (Bioss, Beijing, China) at 37 °C in a cell incubator for 2 h, following the manufacturer's guidelines. Finally, absorbance at 450 nm was measured using a multifunctional microplate reader (Thermofisher, USA).

Western blotting

Treated mouse NPCs were lysed using RIPA lysis solution supplemented with 1/100 of phenylmethylsulfonyl fluoride (Solarbio, Beijing, China). Cellular proteins were extracted through centrifugation at 4 °C, separated

siRNA	sequences (5′–3′)
Si-1	Sense : ACCGAGUGACCGAUUCCAAGUTT Anti-sense: ACUUGGAAUCGGUCACUCGGUTT
Si-2	Sense: GCUGGUGUGUGGACAAGUAUGTT Anti-sense: CAUACUUGUCCACACACCAGCTT
Si-NC	Sense: UUCUCCGAACGUGUCACGUTT Anti-sense: ACGUGACACGUUCGGAGAATT

Table 1. siRNA sequences.

Gene	Primer sequences (5′–3′)
Igfbp3	Forward primer: CCAGGAAACATCAGTGAGTCC Reverse primer: GGATGGAACTTGGAATCGGTCA
Il-6	Forward primer: TAGTCCTTCCTACCCCAATTTCC Reverse primer: TTGGTCCTTAGCCACTCCTTC
Mmp3	Forward primer: ACATGGAGACTTTGTCCCTTTTG Reverse primer: TTGGCTGAGTGGTAGAGTCCC
Cxcl10	Forward primer: CCAAGTGCTGCCGTCATTTTC Reverse primer: GGCTCGCAGGGATGATTTCAA
Ccl2	Forward primer: TTAAAAACCTGGATCGGAACCAA Reverse primer: GCATTAGCTTCAGATTTACGGGT
Nfe2l2	Forward primer: TCTTGGAGTAAGTCGAGAAGTGT Reverse primer: GTTGAAACTGAGCGAAAAAGGC
Gpx3 Sod2 Gapdh	Forward primer: CCTTTTAAGCAGTATGCAGGCA Reverse primer: CAAGCCAAATGGCCCAAGTT Forward primer: CAGACCTGCCTTACGACTATGG Reverse primer: CTCGGTGGCGTTGAGATTGTT Forward primer: AGGTCGGTGTGAACGGATTTG Reverse primer: TGTAGACCATGTAGTTGAGGTCA

Table 2. Primers used in the study.

using ExpressCast PAGE color gels (NCM Bioteth, Suzhou, China), and transferred to polyvinylidene fluoride membranes under constant current. The membranes were blocked using 5% skimmed milk in Tris-buffered saline with Tween-20 at room temperature for 1 h, incubated with primary antibodies overnight at 4 °C, washed three times with TBST, and incubated with secondary antibodies at room temperature. Protein bands were detected using a multicolor fluorescence and chemiluminescence gel imaging system (Bio-Rad, USA). The following antibodies were used in this experiment: anti-Col2a1 (ABclonal, A1560, 1:1000, China), anti-Igfbp3 (Proteintech, 10189-2-AP, 1:500, China), anti-Mmp13 (Servicebio, GB11247-1-100, 1:1000, USA), anti-p21 (Proteintech, 10355-1-AP, 1:1000, USA), anti-p16 (Proteintech, 10883-1-AP, 1:1000, USA), anti-Gapdh (Proteintech, 10494-1-AP, 1:200000, China), anti-mouse and anti-rabbit secondary antibodies (Proteintech, RGAM001/RGAR001, 1:5000, China). Whole uncut membranes were utilized to detect multiple proteins within a single batch of protein samples. Following protein detection using the imaging system, the membrane was stripped using Restore™ PLUS Western Blotting Stripping Buffer (Thermo Fisher Scientific, USA). Once the membrane was thoroughly cleared of primary and secondary antibodies, it was subsequently blocked using 5% skimmed milk and incubated with another primary antibody using a similar procedure to the previous method.

Quantitative real-time PCR analysis
Total RNA was extracted from cells treated with TBHP or luteolin (EZBioscience, USA), according to the manufacturer's instructions. In brief, the cells were washed with PBS and lysed in lysis buffer. An equal volume of anhydrous ethanol was added to the lysed cells, thoroughly mixed, and collected in a centrifuge column for centrifugation at 12,000 rpm in 4 ℃. Then, 500 µL of wash buffer was introduced into the centrifuge column for RNA purification. After centrifugation, the waste liquid in the outer column was discarded, and 20 µL of elution buffer was applied to the inner column. Subsequently, 1 µg of RNA was reverse transcribed into cDNA according to the manufacturer's instructions (Yesen, Shanghai, China). Quantitative real-time PCR (qRT-PCR) was performed in a real-time fluorescence quantitative PCR instrument (Bio-Rad, USA). The sequences of all primers used in this study are detailed in Table 2.

Immunofluorescence
NPCs cultured in confocal Petri dishes were washed three times with precooled PBS, fixed with fresh 4% paraformaldehyde for 15 min, washed with PBS, permeabilized with 0.2% Triton X-100 for 5 min at room temperature, washed with PBS, and blocked with 1% BSA for 1 h at room temperature. Then, cells were incubated with Col2a1 (1:250; Proteintech, Wuhan), or aggrecan (1:500; Proteintech, Wuhan) primary antibodies overnight at 4 °C, followed by incubation with secondary antibodies coupled with fluorescent dyes for 1 h at room temperature away from light. Nuclei were stained with DAPI for 15 min at room temperature away from light. Cells were imaged with a high-resolution laser confocal scanning microscope (LEICA, Germany).

Senescence-associated β-galactosidase staining

For senescence-associated β-galactosidase (SA-β-Gal) staining, NPCs were stained with β-galactosidase following the guidelines provided by the manufacturer (Solarbio, Beijing, China). Briefly, IL-1β- and NAR-treated NPCs cultured in 6-well plates were washed three times with PBS. Subsequently, each well was fixed with 1 mL of β-Gal fixative at room temperature for 15 min, washed three times with PBS, and incubated overnight with β-Gal solution at 37 °C. The cells were observed and imaged using a light microscope (ZEISS, Germany).

Cell proliferation assay

NPCs were subjected to the 5-ethynyl-2′-deoxyuridine (Edu) assay in accordance with the manufacturer's instructions (Beyotime, Shanghai, China). Briefly, an equal volume of Edu reagent was added to IL-1β-treated and NAR-treated NPCs cultured in 96-well plates. The cells were incubated for 2 h at 37 °C in a cell incubator. The culture solution was removed, and the cells were fixed with 4% paraformaldehyde at room temperature for 15 min, washed three times with PBS, incubated with PBS containing 0.3% Triton X-100 at room temperature for 15 min, and washed three times with PBS, and incubated with the click reaction solution for 30 min at room temperature, protected from light. Cells were incubated with Hoechst 33,342 for 10 min at room temperature (shielded from light) to stain nuclei, thoroughly washed with PBS, and observed and imaged using an inverted fluorescence microscope (ZEISS, Germany).

Cell cycle

Cell cycle conditions were examined with a cell cycle analysis kit (Dojindo, Japan), according to the manufacturer's instructions. Drug-treated or transfected cells were stained using a combination of propidium iodide and RNase for 30 min at 4 °C in dark. This was followed by an additional incubation period of 30 min at 37 °C shielded from light. Ultimately, the assessment was performed using flow cytometry equipment (Agilent, USA).

Measurement of intracellular reactive oxygen species

Total intracellular reactive oxygen species (ROS) were detected using ROS Assay Kit-Highly Sensitive DCFH-DA (Dojindo, Japan). Briefly, in cells were treated with drugs or transfections were incubated with a working solution of the highly sensitive DCFH-DA dye for 30 min at 37°C. The cells were thoroughly washed and analyzed by flow cytometry (Agilent, USA) or fluorescence microscopy (ZEISS, Germany).

Statistical analysis

GraphPad Prism 9.0 software was used for statistical analysis. Quantitative data are expressed as the mean ± standard deviation. Two-tailed Student's t test and one-way analysis of variance with the Mann–Whitney test were conducted for statistical analysis. Statistical significance was set at $P < 0.05$.

Results

Identification of DEGs

The datasets GSE56081 and GSE70362 were normalized using the "limma" package in R. Differences between the two datasets caused by different batches and time points were removed using the "sva" package. The datasets were merged into the training group dataset for differential analysis (Fig. 1A,B). In total, 109 DEGs were obtained from the IDD and control groups using the "limma" package in R. Notably, 60 DEGs showed increased expression and 49 had decreased expression. The DEGs were visualized using the "pheatmap" package (Fig. 1C,D).

Enrichment analysis of DEGs

GO enrichment analysis and KEGG enrichment analysis were conducted on 109 DEGs to elucidate their function. GO analysis revealed enrichment in biological processes, such as positive regulation of angiogenesis, positive regulation of vasculature development, collagen fibril organization, negative regulation of osteoblast differentiation, regulation of angiogenesis, lymph vessel development, regulation of vasculature development, and cartilage development (Fig. 2A). KEGG analysis showed enrichment in signaling pathways, including mineral absorption, transcriptional misregulation in cancer, p53 signaling pathway, glycosphingolipid biosynthesis—lacto and neolacto series, *Staphylococcus aureus* infection, protein digestion and absorption, tryptophan metabolism, and pyruvate metabolism (Fig. 2B).

Identification of diagnostic markers in IDD

To acquire diagnostic marker genes for IDD, we analyzed 109 DEGs using LASSO and SVM (Fig. 3). LASSO identified 15 genes most strongly correlated with IDD: MED11, MGP, CYP1B1, BTG2, EMILIN1, MROH1, GREM1, ITGB1BP1, EFNB2, SLC16A3, LDHC, LRRC10B, NOS1AP, PWAR6, and IGFBP3 (Fig. 3A,B). By contrast, SVM identified 11 genes closely linked to IDD: MED11, IGFBP3, CYP1B1, SLC16A3, BTG2, PWAR6, EMILIN1, LDHC, MT1F, STARD10, and LRRC10B (Fig. 3C,D).

Identification and validation of core genes

To identify core genes, we initially acquired 502 ARGs from The Aging Gene Database (Fig. 4A). Merging targets sourced from the TCMSP Database, DrugBank Database, STITCH Database, and SwissTargetPrediction database yielded 142 targets associated with NAR (Fig. 4A). The intersection of 502 ARGs, 142 NAR-related targets, and diagnostic marker genes yielded IGFBP3 (Fig. 4A). R language was used to examine differential expression of IGFBP3 in training and verification group datasets. IGFBP3 expression was substantially upregulated in the IDD group (Fig. 4B,C). The ROC curve validated the diagnostic efficacy of IGFBP3 (AUC > 0.7), signifying notable diagnostic value of IGFBP3 for IDD (Fig. 4D).
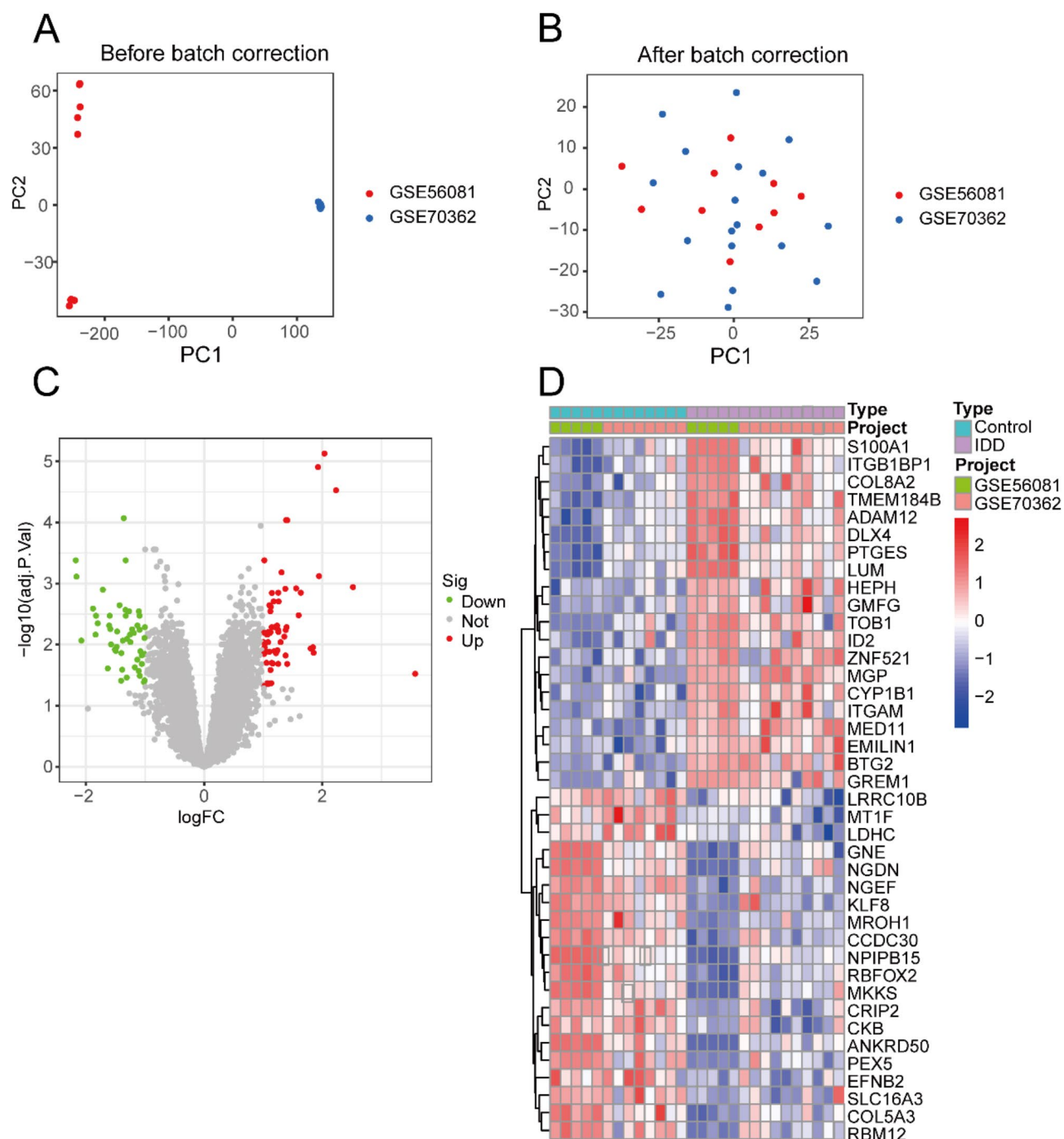
Fig. 1. Datasets preprocessing and differential expression. (**A**) Distribution of merged data before batch correction. (**B**) Distribution of merged data after batch correction. (**C**) Volcano and (**D**) Heatmaps of genes differentially expressed in merged datasets after batch correction. *IDD* Intervertebral disc degeneration.

Igfbp3 expression was upregulated in IL-1β-induced NPCs in senescence and degeneration

In the context of an IL-1β-induced cellular senescence and degeneration model, we validated the differential expression of Igfbp3. We used Col2a1 as an IF marker and identified primary NPCs, each showing unique Col2a1 expression (Fig. 5A). IL-1β treatment revealed significant findings: Igfbp3, P21, P16, and Mmp13 expression increased and Col2a1 expression decreased with increasing IL-1β concentration (Fig. 5B). At 20 ng/mL, IL-1β induced significant protein alterations, leading to its selection for subsequent experiments. Furthermore, we explored the effect of IL-1β on NPCs, evaluating SA-β-Gal activity and conducting immunofluorescence analysis. The results demonstrated that IL-1β substantially increased SA-β-Gal activity (Fig. 5C) and decreased aggrecan expression (Fig. 5D). Collectively, these findings indicate that IL-1β-induced NPCs exhibit clear
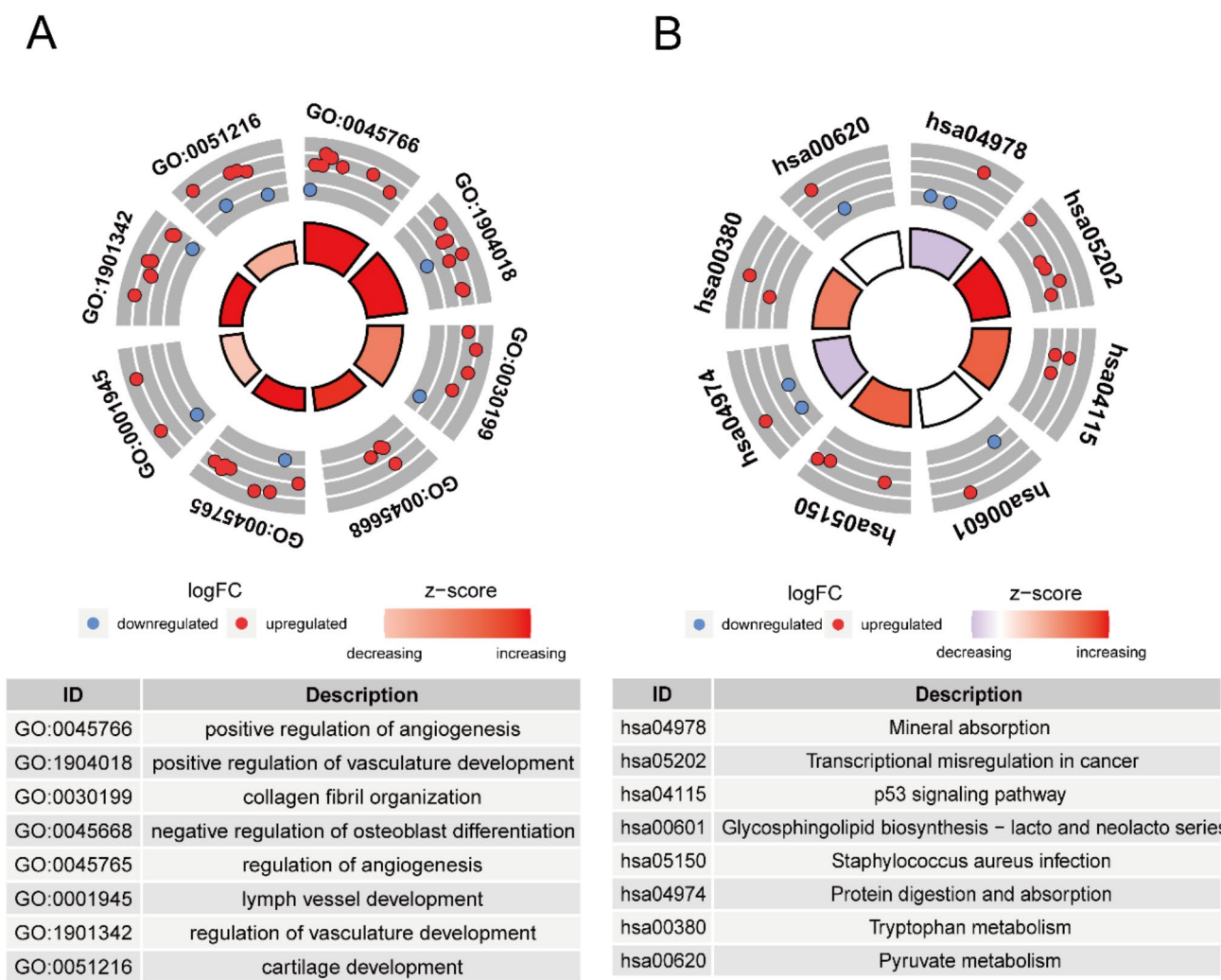
Fig. 2. Functional enrichment analysis of DEGs. (**A**) Results of GO enrichment. (**B**) Results of KEGG enrichment.

signs of cellular aging and degeneration in vitro, accompanied by increased Igfbp3 expression in the aging and degenerating NPCs.

Igfbp3 knockdown alleviates IL-1β-induced senescence and degeneration of NPCs

To investigate the influence of Igfbp3 on senescence and degeneration in IL-1β-induced NPCs, we used siRNA to suppress Igfbp3 expression in NPCs. We found that si-1 had the highest efficiency in suppressing Igfbp3 mRNA and protein expression (Fig. 6A,B) and used it for subsequent experiments. NPCs were treated with 20 ng/mL IL-1β or si-1. Western blot analysis to examine the expression of proteins associated with senescence markers and ECM balance showed that Igfbp3 depletion decreased P21, P16, and Mmp13 expression and increased Col2a1 expression (Fig. 6C). Additionally, Igfbp3 suppression enhanced NPC proliferation (Fig. 6D) and reduced SA-β-Gal activity (Fig. 6E).

Binding of NAR to IGFBP3

NAR, an intrinsic flavanone with a molecular formula of $C_{15}H_{12}O_5$ (Fig. 7A), was evaluated for its binding to IGFBP3. This assessment involved molecular docking at the active site of IGFBP3, followed by subsequent MM-GBSA computational analysis. The docking results revealed an MM-GBSA dG Bind of -27.82 kcal/mol, indicating low binding free energy. NAR was found to bind to the active pocket surface of IGFBP3, making hydrophobic interactions with LEU139, ALA138, LEU134, LEU110, and LEU137 and forming hydrogen bonds with GLU162, SER136, SER112, and LEU113 (Fig. 7B,C). Results of the CCK-8 assay indicated that < 50 μM NAR had no discernible impact on NPC viability (Fig. 7D). Therefore, subsequent experiments were conducted using 50 μM NAR.
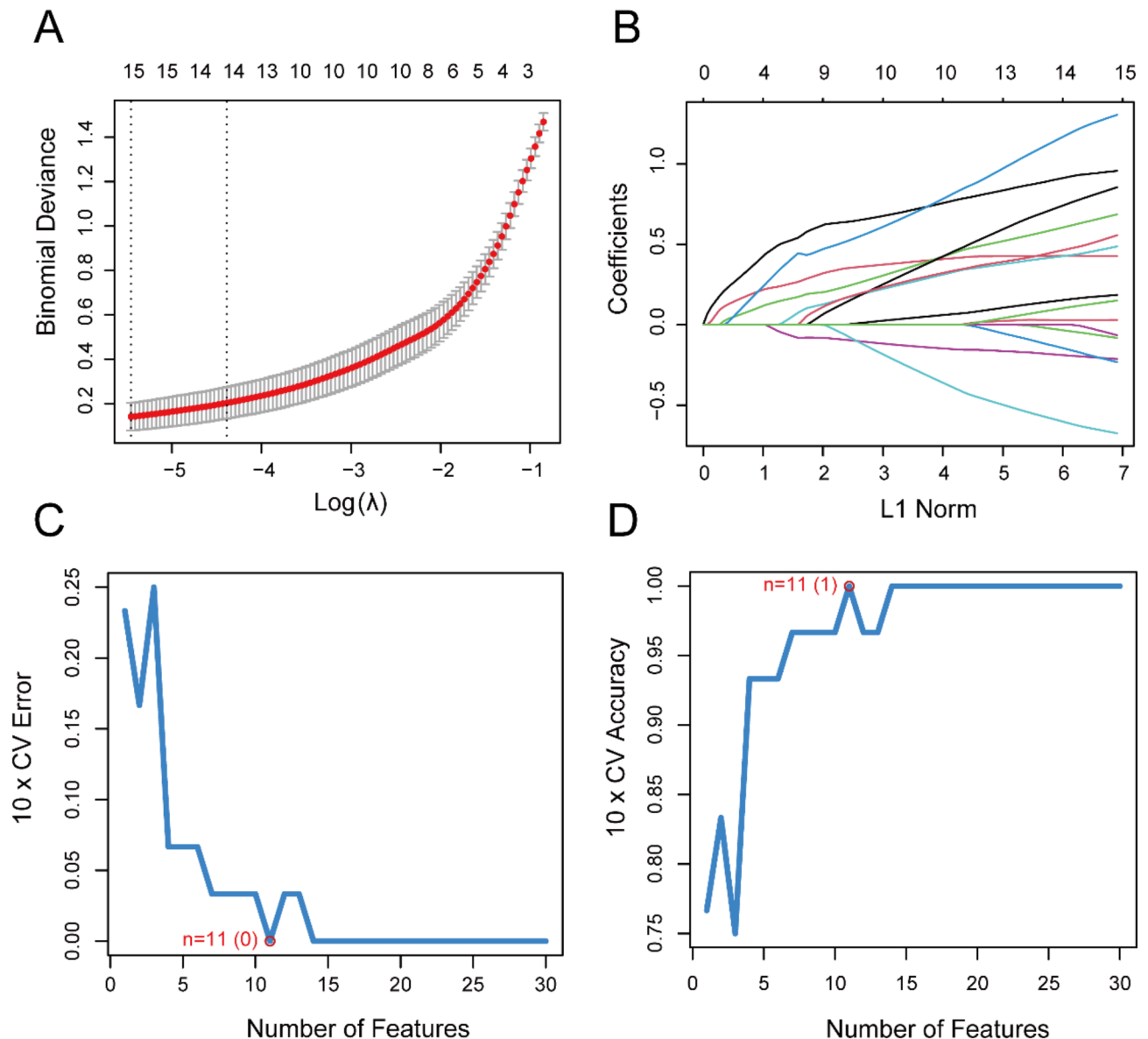
Fig. 3. Screening for diagnostic marker genes by machine learning. (**A,B**) Results of the lasso screening. (**C,D**) Results of the SVM screening.

NAR reduced Igfbp3 expression and alleviated IL-1β-induced NPC senescence and degeneration

Treatment of NPCs with 20 ng/mL IL-1β or two concentrations of NAR (25 or 50 μM) reduced Igfbp3 expression and mitigated IL-1β-induced senescence and degeneration. This reduction was concentration dependent and correlated with decreased expression of Igfbp3/Mmp13 and senescence-associated proteins P16/P21, coupled with an increase in Col2a1 expression (Fig. 8A). Furthermore, we observed alleviation of IL-1β-induced inhibition of cellular proliferation (Fig. 8B), increase in aggrecan expression (Fig. 8C), reduction in the expression of SASP genes (Il-6, Mmp3, Cxcl10, and Ccl2) (Fig. 8D), and attenuation of G0/G1 cell cycle arrest (Fig. 9).

NAR reduced ROS production and increased antioxidant enzyme activity

Excessive levels of ROS can lead to significant oxidative damage, accelerating aging[43]. ROS-induced cellular senescence and apoptosis are crucial factors in the development of IDD[44]. Considering this, our investigation aimed to determine whether NAR could inhibit ROS production and provide a protective effect. Flow cytometry results demonstrated that IL-1β substantially increased intracellular ROS generation, whereas NAR significantly reduced overall ROS production (Fig. 10A). Regulation of the enzymatic antioxidant system is vital for maintaining ROS homeostasis[42]. Our qRT-PCR results revealed that IL-1β significantly downregulated the expression of antioxidant enzyme-related genes (Nfe2l2, Gpx3, and Sod2), with NAR partially restoring the expression of these genes (Fig. 10B).
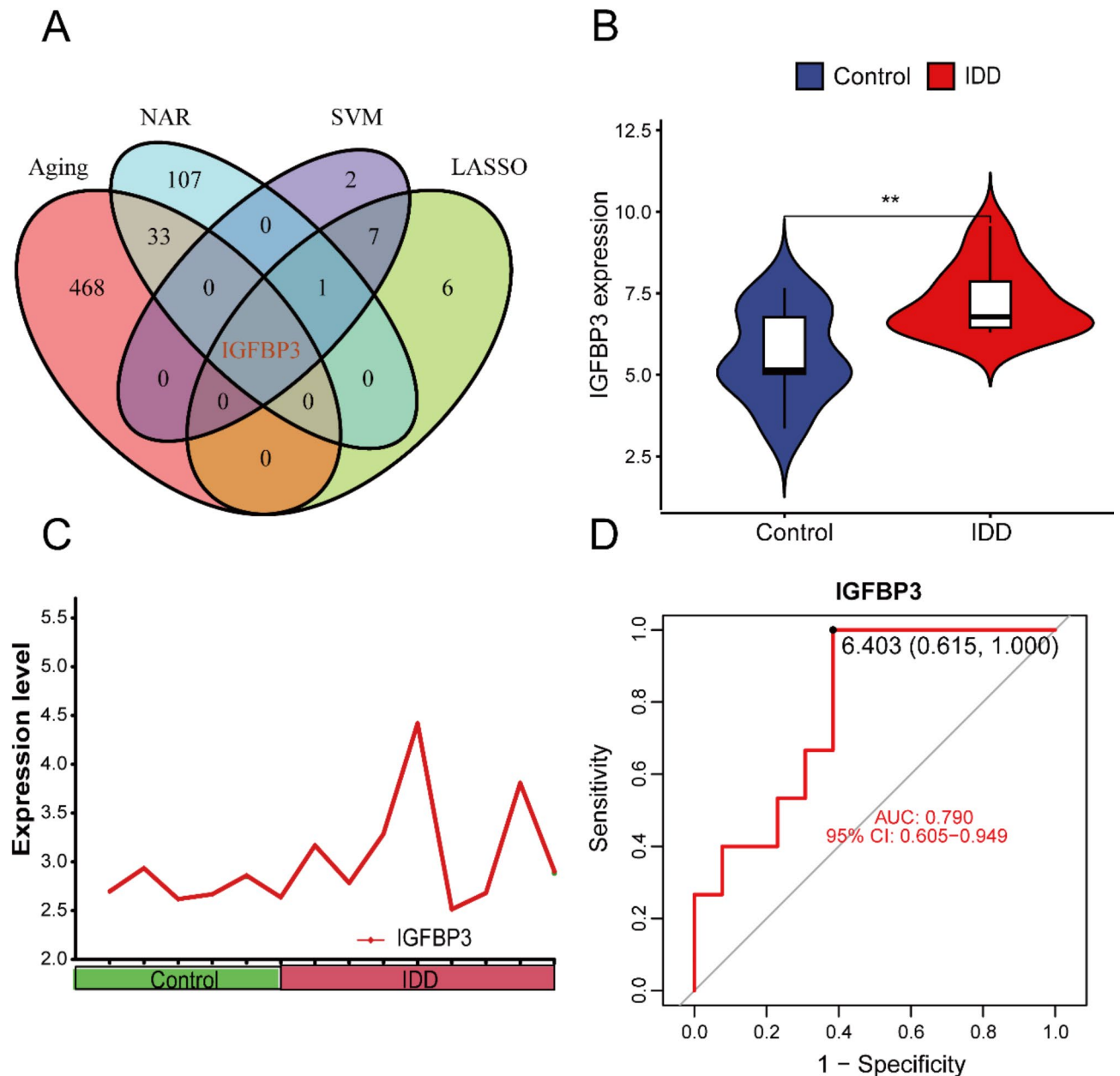
Fig. 4. Identification and validation of core genes. (**A**) Core genes are screened by taking the intersection of ARGs, NAR-related targets, and diagnostic marker genes from machine learning screening. (**B**) Validation of differential expression of the core gene IGFBP3 in the training set dataset. (**C**) Differential expression of the core gene IGFBP3 in the validation set dataset. (**D**) Validation of the diagnostic efficiency of IGFBP3.

IGFBP3 reduced the therapeutic potential of NAR in addressing cellular senescence and degeneration

Treatment with standard concentrations of IL-1β (20 ng/mL) and recombinant IGFBP3 (50 ng/mL) or NAR (50 μM) showed that NAR inhibited the expression of Mmp13 and P21/P16 and promoting Col2a1 expression. However, recombinant IGFBP3 weakened this effect by increasing the expression of Mmp13 and P21/P16 and decreasing Col2a1 expression (Fig. 11A). Additionally, recombinant IGFBP3 impaired the ability of NAR to inhibit the activity of SA-β-Gal (Fig. 11B) and promote aggrecan expression (Fig. 11C).

Discussion

IDD significantly contributes to the deterioration of quality-of-life and onset of chronic debilitation in middle-aged and elderly individuals[46–48]. Studies have revealed that IDD onset and progression are influenced by various factors, including aging, oxidative stress, inflammation, genetics, and the dynamic environment[49]. The diagnosis of IDD relies on a combination of diagnostic imaging techniques and clinical symptomatology[50]. However, the early stages of the disease are usually asymptomatic; therefore, patients with IDD are usually diagnosed in
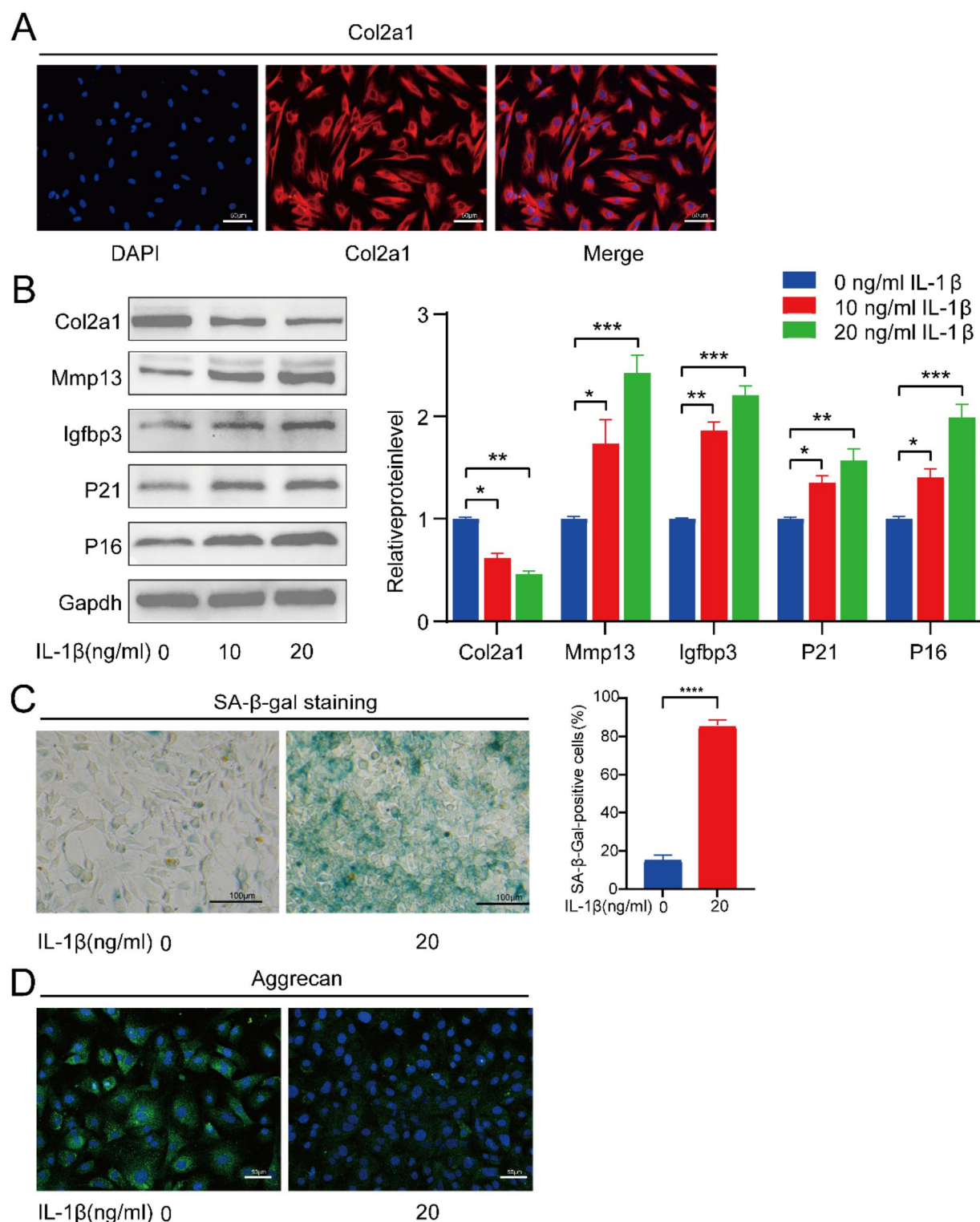
Fig. 5. Modeling of cellular senescence and degeneration and expression of Igfbp3 protein. (**A**) Identification of NPCs. (**B**) Western blot analysis of Col2a1, Mmp13, Igfbp3,P21 and P16 protein levels in NPCs treated with different concentrations of IL-1β. (**C**) SA-β-Gal staining of NPCs treated with or without.

the later stages[51]. The identification of genetic markers with diagnostic potential holds great promise for early detection and intervention in IDD, surpassing the dependence on radiological examinations[52]. Consequently, the application of bioinformatics to analyze genomic data for the identification of diagnostic genetic markers is promising.
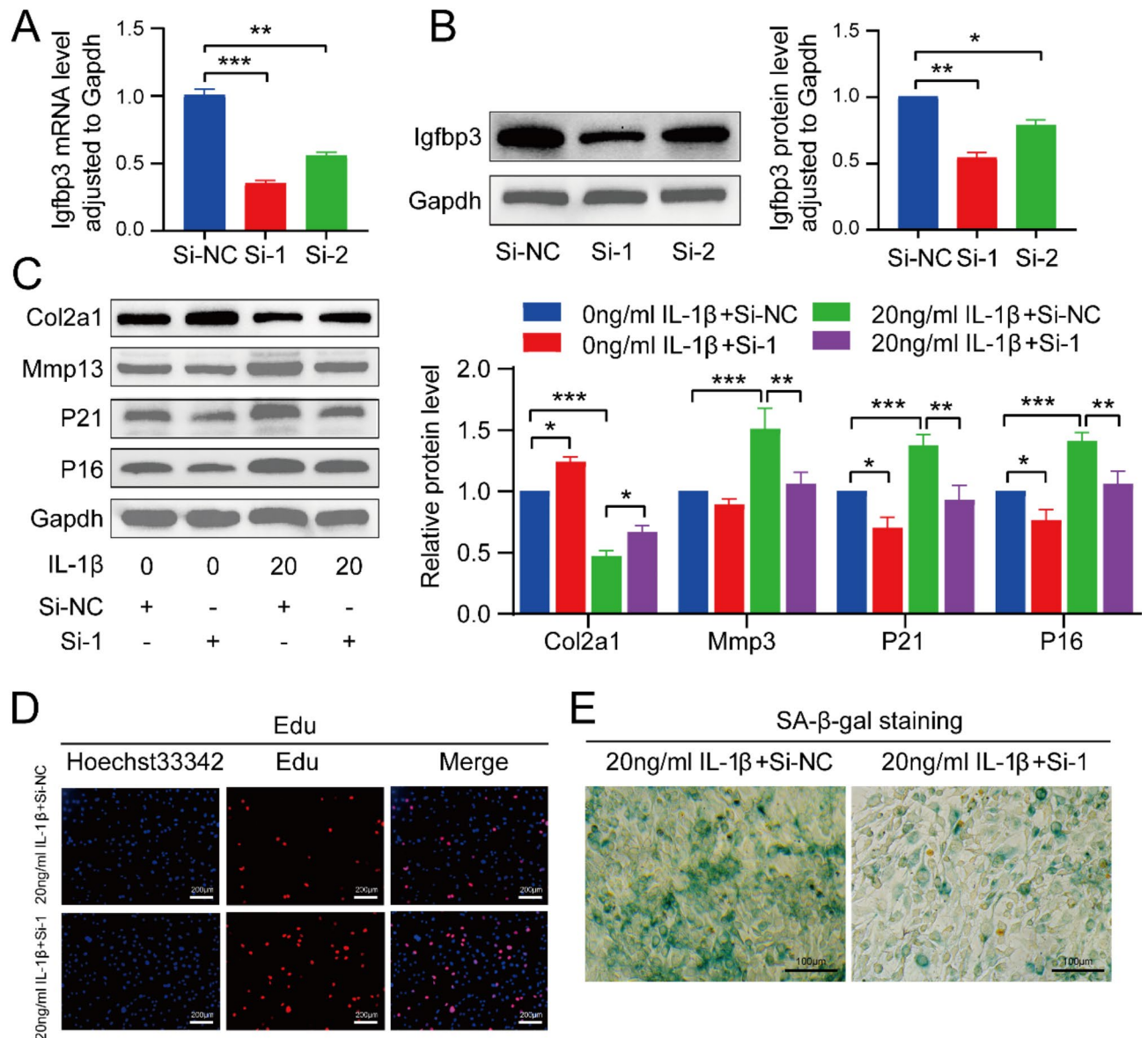
Fig. 6. Knockdown of Igfbp3 alleviates IL-1β-induced senescence and degeneration of NPCs. (**A**) qRT-PCR analysis of Igfbp3 expression levels after transfection of NPCs with siRNA. (**B**) WB analysis of Igfbp3 expression levels after transfection of NPCs with siRNA. (**C**) Changes in the ECM markers Col2a1 or Mmp13 and the senescence markers P21 or P16 after transfection with siRNA were confirmed by WB. (**D**) Effect of transfection with siRNA on the proliferation of NPCs. Scare bar = 200 μm. (**E**) Effect of transfection with siRNA on the SA-β-Gal activity of NPCs. Scare bar = 100 μm.

Differential analysis of the training group dataset identified 60 DEGs with increased expression and 49 DEGs with decreased expression in the context of IDD. GO enrichment analysis of the 109 DEGs showed notable enrichment promoting angiogenesis, organizing collagen fibrils, and developing cartilage. Angiogenesis plays a critical role in repairing degenerated IVDs[53]. Zeldin et al. utilized second harmonic generation imaging and sophisticated image processing algorithms to quantify collagen in the IVD, establishing a strong correlation between collagen fibril organization and IDD[54]. KEGG analysis showed that the DEGs had a close relationship with *S. aureus* infection and p53 signaling. *S. aureus* infection within the IVD accelerated IDD progression[55–57], whereas inhibition of P53 significantly slowed IDD progression[58]. In addition, diagnostic marker genes identified by LASSO regression and SVM were intersected with 142 NAR targets and 502 ARGs. IGFBP3 was selected as the core gene for this study. Differential analysis of the training and validation group datasets indicated an increase in IGFBP3 expression in IDD. The diagnostic efficacy of IGFBP3 was evaluated through ROC curve analysis, revealing its significant diagnostic accuracy.

The progression of IDD is intricately linked to the IL-1β-induced inflammatory response[59]. As a member of the IL-1 family, IL-1β exhibits potent proinflammatory properties, initiating the production of various proinflammatory factors[60]. Moreover, IL-1β expedites IDD advancement by contributing to ECM degradation[61]
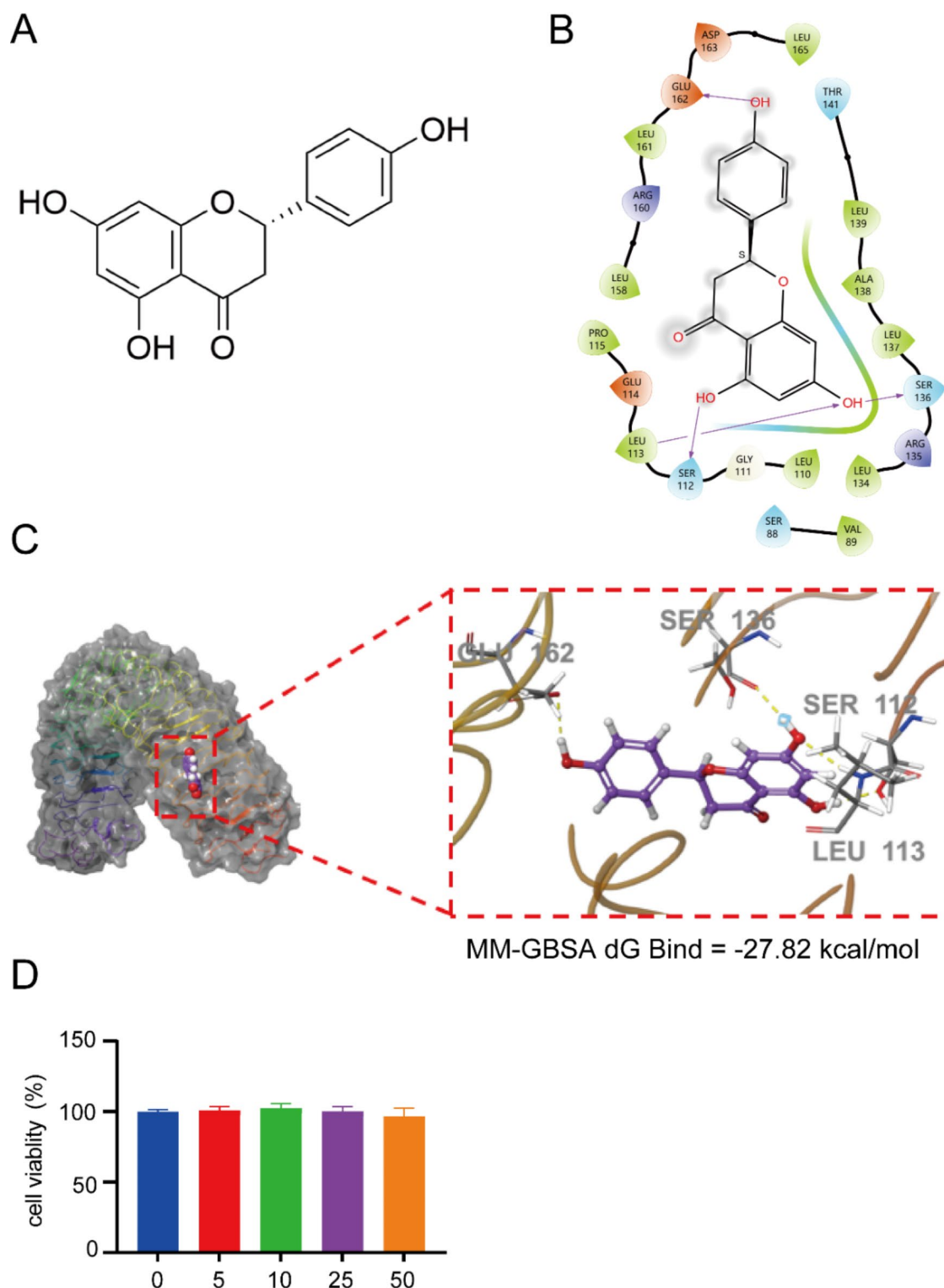
Fig. 7. Binding of NAR to Igfbp3 and the effect of NAR on cell viability. (**A**) Molecular structure of NAR. (**B**) 2D structure of NAR binding to Igfbp3. (**C**) 3D structure of NAR binding to Igfbp3. (**D**) Effect of different concentrations of NAR on the viability of NPCs.

and NPC senescence[62,63]. In this study, IL-1β functioned as a highly effective inducer of senescence and degeneration in NPCs. This was substantiated by the reduced expression of Col2a1/aggrecan proteins, increased expression of P21/P16/Mmp13 proteins, and elevated SA-β-gal activity consistent with increasing IL-1β concentration. Comparison of normal NPCs with their senescent and degenerating counterparts revealed that
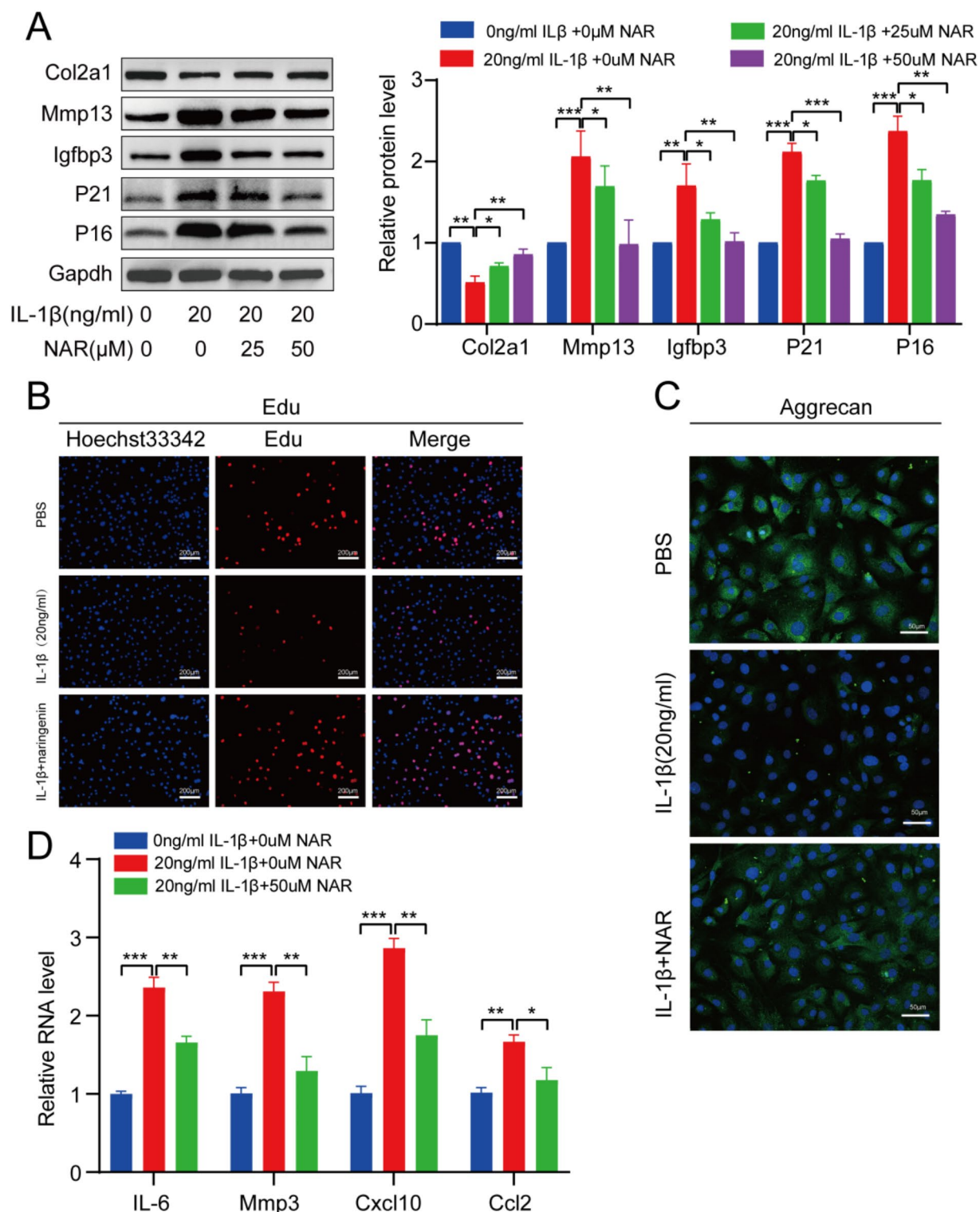
Fig. 8. Effect of NAR on Igfbp3 protein expression and the senescence and degeneration phenotype of NPCs. (**A**) WB detected changes in the expression levels of Col2a1, Mmp13 Igfbp3, P21 and P16 after treatment of NPCs with NAR. (**B**) Changes in cell proliferation after NAR treatment of NPCs. Scare bar = 200 μm. (**C**) Changes in Aggrecan after NAR treatment of NPCs Scare bar = 50 μm. (**D**) Expression of SASP-related genes Il-6, Mmp3, Cxcl10 and Ccl2 after NAR treatment of NPCs detected by qRT-PCR.
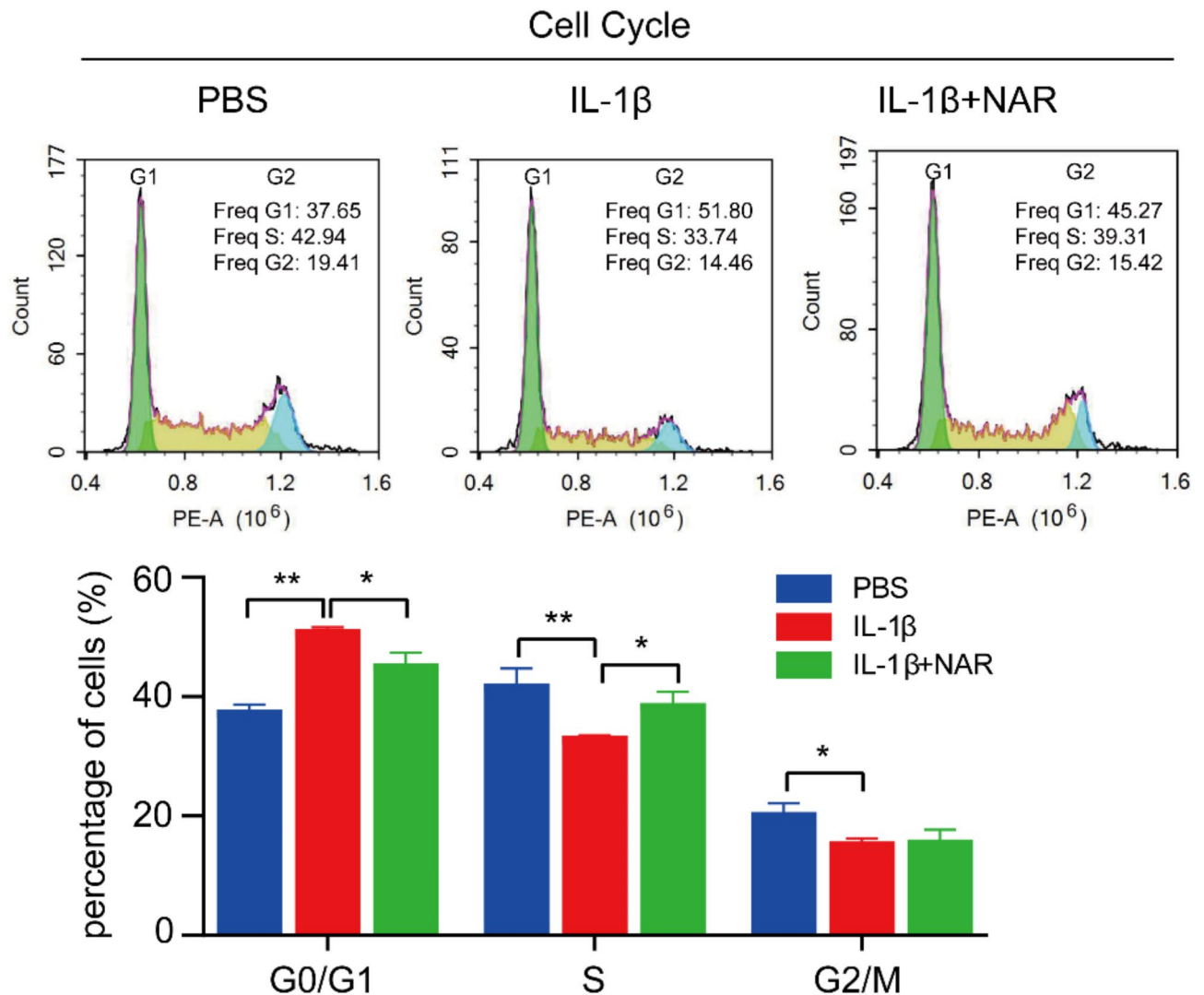
Fig. 9. Effect of NAR on the cell cycle.

Igfbp3 expression was more pronounced in senescent and degenerating NPCs than normal NPCs. This finding further supports the results of our bioinformatics analysis.

IGFBP3 is a versatile protein with a pivotal role in promoting aging[64]. Owing to its antiproliferative and proapoptotic properties, it induces apoptosis in various cell types[65,66]. As a component of the SASP, IGFBP3 expression is elevated in senescent cells[67]. Cellular senescence, the fundamental contributor to aging, is intimately linked to chronic ailments in the cardiovascular, musculoskeletal, and neurological systems[68–71]. Notably, cellular senescence significantly contributes to the progression of IDD[72]. Senescent cells release cytokines, enzymes, growth factors, and chemokines, inciting inflammatory responses and catabolic processes that exacerbate IDD[73,74]. Our investigation aimed to elucidate the role of IGFBP3 in the IL-1β-induced senescence and degeneration of NPCs. We silenced *Igfbp3* expression using siRNA. Knockdown of Igfbp3 protein in NPCs with IL-1β-induced senescence and degeneration caused a decrease in the expression of Mmp13/P21/P16 proteins and reduced SA-β-gal activity, with a simultaneous increase in Col2a1 expression and cell proliferation. These findings strongly indicate that IGFBP3 functions as a pathological factor contributing to the promotion of degeneration and senescence in NPCs.

Pharmacological interventions for IDD primarily target al.leviating clinical symptoms. Nevertheless, this approach cannot control or reverse IDD progression[13]. Hence, the imperative lies in developing pharmaceuticals capable of preventing or ameliorating IDD progression. Recently, studies have highlighted natural herbal extracts for their antiaging and anti-inflammatory properties[75,76]. Network pharmacology and bioinformatics analysis showed that IGFBP3 is a common target of NAR, aging, and IDD. We postulate that NAR exerts its therapeutic influence on aging and degeneration in NPCs by modulating IGFBP3. Initially, molecular docking demonstrated a notably low binding free energy between NAR and IGFBP3. Subsequently, in senescent and degenerating NPCs, NAR demonstrated inhibition of Mmp13, P21, P16, and Igfbp3 expression, suppression of SASP-related gene expression, promotion of Col2a1 and aggrecan expression, and promotion of cell proliferation. NAR exhibited antioxidative properties by inhibiting total ROS production and enhancing antioxidant enzyme gene expression.
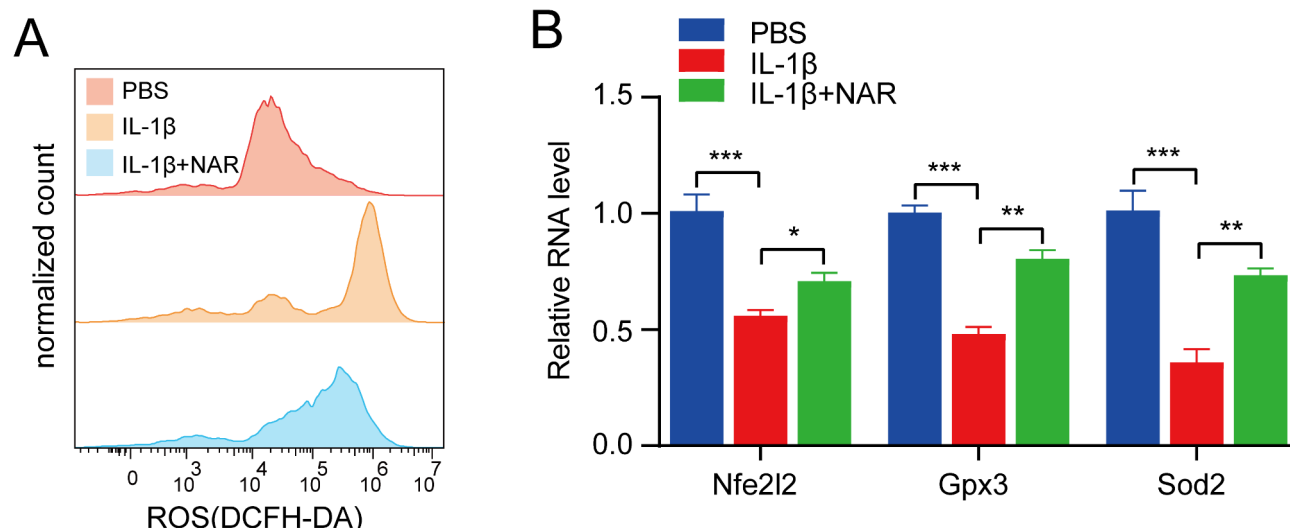
Fig. 10. Effect of NAR on ROS and antioxidant enzyme systems. (**A**) Effect of NAR on total intracellular ROS in NPCs detected by flow cytometry. (**B**) qRT-PCR assay confirmed that NAR promoted the expression of antioxidant enzyme-related genes Nfe2l2, Gpx3 and Sod2 in NPCs.

Rescue experiments were performed to investigate whether the antiaging and antidegenerative properties of NAR are mediated by inhibiting Igfbp3 expression. Our findings showed that introducing recombinant IGFBP3 markedly diminished the therapeutic efficacy of NAR. These findings offer insights into the role of NAR in aging and degeneration, shedding light on potential avenues for IDD prevention and treatment.

This study has several limitations that necessitate consideration when interpreting the results. First, the two datasets were standardized independently. Following this, the standardized data were merged, and batch effects in the combined dataset were corrected using the "SVA" batch effect correction algorithm, thereby enhancing the consistency among the samples. To further validate the accuracy of the differential analysis results, we conducted differential analysis on independent samples. The findings indicated that the results from the training group were consistent with those from the validation group. This result was further corroborated in subsequent cellular experiments. However, inherent differences between batches still persist, which may elevate the risk of false positives (incorrectly identified as significant) or false negatives (overlooking true significance). To mitigate this issue, future studies will incorporate a random effects model, employ multiple batch effect correction algorithms, and gather a larger number of samples from the same batch for bioinformatics analysis. Second, the functional roles of NAR and IGFBP3 were confirmed through cellular experiments, highlighting the need for further in vivo validation. Third, molecular docking techniques were used to confirm binding between NAR and IGFBP3, and direct confirmation of binding is lacking. Future efforts will focus on additional validation through Biacore analysis and pull-down assays.

Conclusion

This study combines network pharmacology and bioinformatics to elucidate the anti-aging and anti-degenerative effects of NAR on NPCs through IGFBP3 targeting. Additionally, using an in vitro cellular model of aging and degeneration in NPCs, we discovered that NAR mitigates the aging and degeneration process by downregulating Igfbp3 expression. Collectively, these findings offer valuable insights into understanding the mechanism of action of NAR and identifying preventive and therapeutic strategies for IDD.
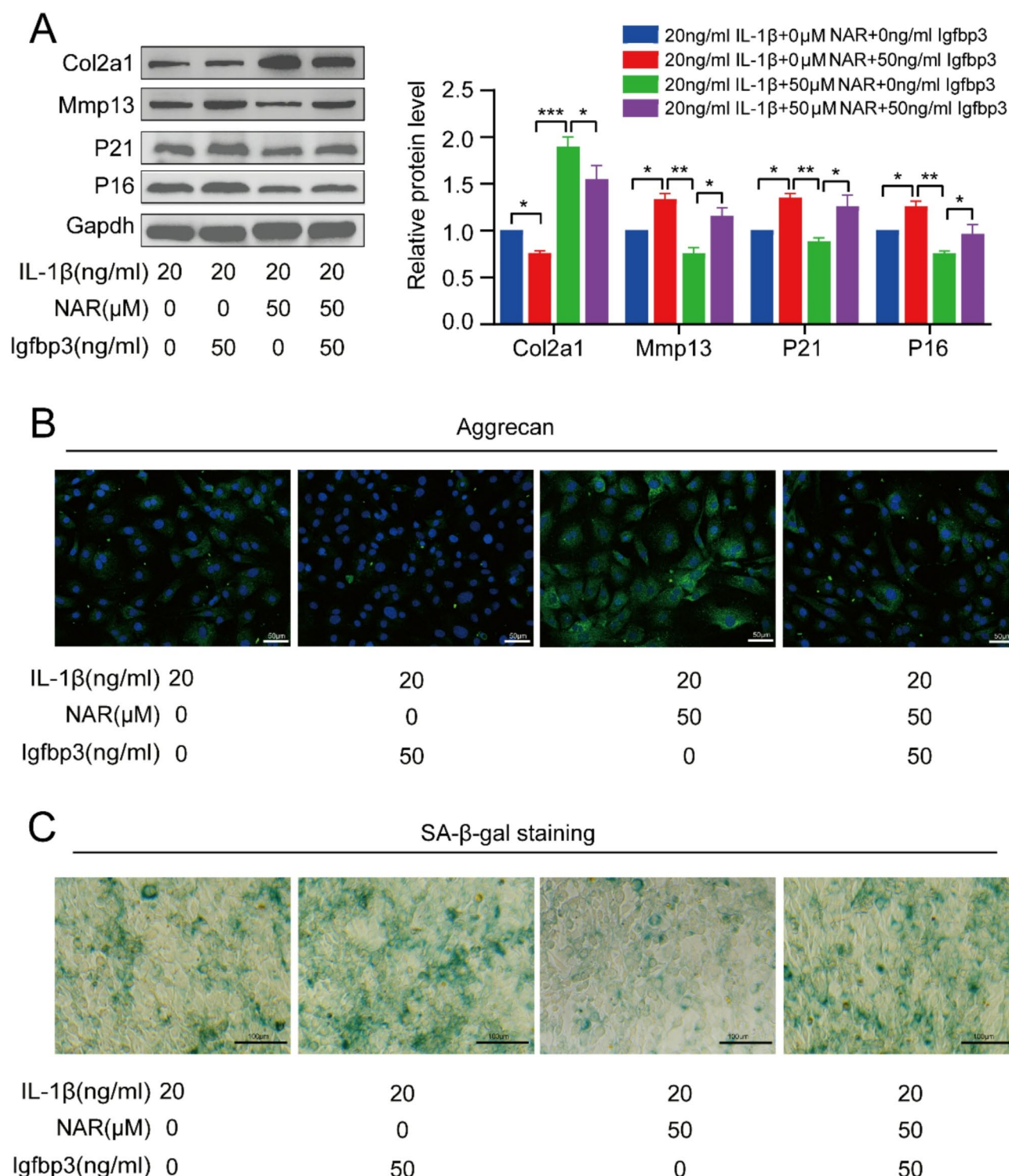
Fig. 11. Igfbp3 protein weakened NAR anti-aging and anti-degeneration capacity. (**A**) WB assay of recombinant IGFBP3 protein on Col2a1, Mmp13, P21 and P16 proteins. (**B**) Immunofluorescence detection of the effect of recombinant IGFBP3 protein on Aggrecan. Scare bar = 50 μm. (**C**) Effect of recombinant IGFBP3 protein on SA-β-Gal activity. Scare bar = 100 μm.

Data availability

www.swisstargetprediction.ch) and The Aging Gene Database (https://www.genomics.senescence.info/genes/index.html).

References

1. Priyadarshani, P., Li, Y. & Yao, L. Advances in biological therapy for nucleus pulposus regeneration. *Osteoarthr. Cartil.* **24**, 206–212. https://doi.org/10.1016/j.joca.2015.08.014 (2016).
2. Gatchel, R. J. The continuing and growing epidemic of chronic low back pain. *Healthc. (Basel).* **3**, 838–845. https://doi.org/10.3390/healthcare3030838 (2015).
3. Diwan, A. D. & Melrose, J. Intervertebral disc degeneration and how it leads to low back pain. *JOR Spine.* **6**, e1231. https://doi.org/10.1002/jsp2.1231 (2023).
4. Sampara, P., Banala, R. R., Vemuri, S. K., Av, G. R. & Gpv, S. Understanding the molecular biology of intervertebral disc degeneration and potential gene therapy strategies for regeneration: a review. *Gene Ther.* **25**, 67–82. https://doi.org/10.1038/s41434-018-0004-0 (2018).
5. Ma, K. et al. Mechanisms of endogenous repair failure during intervertebral disc degeneration. *Osteoarthr. Cartil.* **27**, 41–48. https://doi.org/10.1016/j.joca.2018.08.021 (2019).
6. Ren, B. O., Khambete, P., Rasendran, C., O'Donnell, J. A. & Ahn, N. U. Quantifying the economic impact of depression for spine patients in the United States. *Clin. Spine Surg.* **35**, E374–E379. https://doi.org/10.1097/BSD.0000000000001220 (2022).
7. Yong, R. J., Mullins, P. M. & Bhattacharyya, N. Prevalence of chronic pain among adults in the United States. *Pain* **163**, e328–e332. https://doi.org/10.1097/j.pain.0000000000002291 (2022).
8. Ashinsky, B., Smith, H. E., Mauck, R. L. & Gullbrand, S. E. Intervertebral disc degeneration and regeneration: a motion segment perspective. *Eur. Cell. Mater.* **41**, 370–380. https://doi.org/10.22203/eCM.v041a24 (2021).
9. Desmoulin, G. T., Pradhan, V. & Milner, T. E. Mechanical aspects of intervertebral disc Injury and implications on Biomechanics. *Spine (Phila Pa. 1976).* **45**, E457–E464. https://doi.org/10.1097/BRS.0000000000003291 (2020).
10. Zhang, Z. et al. PLK1 mitigates intervertebral disc degeneration by delaying senescence of Nucleus Pulposus cells. *Front. Cell. Dev. Biol.* **10**, 819262. https://doi.org/10.3389/fcell.2022.819262 (2022).
11. Zhang, G. Z. et al. BRD4 inhibition suppresses senescence and apoptosis of Nucleus Pulposus cells by inducing autophagy during intervertebral disc degeneration: an in Vitro and in vivo study. *Oxid. Med. Cell. Longev.* **2022** (9181412). https://doi.org/10.1155/2022/9181412 (2022).
12. Dou, Y., Sun, X., Ma, X., Zhao, X. & Yang, Q. Intervertebral disk degeneration: the microenvironment and tissue engineering strategies. *Front. Bioeng. Biotechnol.* **9**, 592118. https://doi.org/10.3389/fbioe.2021.592118 (2021).
13. Lyu, F. J. et al. IVD progenitor cells: a new horizon for understanding disc homeostasis and repair. *Nat. Rev. Rheumatol.* **15**, 102–112. https://doi.org/10.1038/s41584-018-0154-x (2019).
14. Moriguchi, Y. et al. Biological treatment approaches for degenerative disk disease: a literature review of in vivo animal and clinical data. *Glob. Spine J.* **6**, 497–518. https://doi.org/10.1055/s-0036-1571955 (2016).
15. Kamali, A. et al. Small molecule-based treatment approaches for intervertebral disc degeneration: current options and future directions. *Theranostics* **11**, 27–47. https://doi.org/10.7150/thno.48987 (2021).
16. Herranz, N. & Gil, J. Mechanisms and functions of cellular senescence. *J. Clin. Investig.* **128**, 1238–1246. https://doi.org/10.1172/JCI95148 (2018).
17. Mehdizadeh, M., Aguilar, M., Thorin, E., Ferbeyre, G. & Nattel, S. The role of cellular senescence in cardiac disease: basic biology and clinical relevance. *Nat. Rev. Cardiol.* **19**, 250–264. https://doi.org/10.1038/s41569-021-00624-2 (2022).
18. Wu, Y. et al. Senolytics: eliminating senescent cells and alleviating intervertebral disc degeneration. *Front. Bioeng. Biotechnol.* **10**, 823945. https://doi.org/10.3389/fbioe.2022.823945 (2022).
19. Wu, J. et al. Self-amplifying loop of NF-kappaB and periostin initiated by PIEZO1 accelerates mechano-induced senescence of nucleus pulposus cells and intervertebral disc degeneration. *Mol. Ther.* **30**, 3241–3256. https://doi.org/10.1016/j.ymthe.2022.05.021 (2022).
20. Cheng, F. et al. The role of oxidative stress in intervertebral disc cellular senescence. *Front. Endocrinol. (Lausanne).* **13**, 1038171. https://doi.org/10.3389/fendo.2022.1038171 (2022).
21. Lu, X. D., Liu, Y. R. & Zhang, Z. Y. Matrilin-3 alleviates extracellular matrix degradation of nucleus pulposus cells via induction of IL-1 receptor antagonist. *Eur. Rev. Med. Pharmacol. Sci.* **24**, 5231–5241. https://doi.org/10.26355/eurrev_202005_21305 (2020).
22. Yang, W. et al. Interleukin-1beta in intervertebral disk degeneration. *Clin. Chim. Acta.* **450**, 262–272. https://doi.org/10.1016/j.cca.2015.08.029 (2015).
23. Zaidun, N. H., Thent, Z. C. & Latiff, A. A. Combating oxidative stress disorders with citrus flavonoid: Naringenin. *Life Sci.* **208**, 111–122. https://doi.org/10.1016/j.lfs.2018.07.017 (2018).
24. Den Hartogh, D. J. & Tsiani, E. Antidiabetic properties of naringenin: a citrus fruit polyphenol. *Biomolecules* **9**. https://doi.org/10.3390/biom9030099 (2019).
25. Zeng, W., Jin, L., Zhang, F., Zhang, C. & Liang, W. Naringenin as a potential immunomodulator in therapeutics. *Pharmacol. Res.* **135**, 122–126. https://doi.org/10.1016/j.phrs.2018.08.002 (2018).
26. Patel, K., Singh, G. K. & Patel, D. K. A review on pharmacological and analytical aspects of Naringenin. *Chin. J. Integr. Med.* **24**, 551–560. https://doi.org/10.1007/s11655-014-1960-x (2018).
27. Salehi, B. et al. The therapeutic potential of naringenin: a review of clinical trials. *Pharmaceuticals (Basel).* **12** https://doi.org/10.3390/ph12010011 (2019).
28. Yang, Y., Trevethan, M., Wang, S. & Zhao, L. Beneficial effects of citrus flavanones naringin and naringenin and their food sources on lipid metabolism: an update on bioavailability, pharmacokinetics, and mechanisms. *J. Nutr. Biochem.* **104**, 108967. https://doi.org/10.1016/j.jnutbio.2022.108967 (2022).
29. Pan, Z. et al. Naringenin protects against iron overload-induced osteoarthritis by suppressing oxidative stress. *Phytomedicine* **105**, 154330. https://doi.org/10.1016/j.phymed.2022.154330 (2022).
30. Wang, J., Wu, R., Hua, Y., Ling, S. & Xu, X. Naringenin ameliorates vascular senescence and atherosclerosis involving SIRT1 activation. *J. Pharm. Pharmacol.* **75**, 1021–1033. https://doi.org/10.1093/jpp/rgad053 (2023).
31. Al-Rejaie, S. S. et al. Protective effect of naringenin on acetic acid-induced ulcerative colitis in rats. *World J. Gastroenterol.* **19**, 5633–5644. https://doi.org/10.3748/wjg.v19.i34.5633 (2013).
32. Zhao, L. et al. Network pharmacology, a promising approach to reveal the pharmacology mechanism of Chinese medicine formula. *J. Ethnopharmacol.* **309**, 116306. https://doi.org/10.1016/j.jep.2023.116306 (2023).
33. Annie Lee, E. S., Zhou, P. & Wong, A. K. C. In *Bioinformatics* (ed Helder, I. N.) (2021).
34. Ru, J. et al. TCMSP: a database of systems pharmacology for drug discovery from herbal medicines. *J. Cheminform.* **6**, 13. https://doi.org/10.1186/1758-2946-6-13 (2014).
35. Daina, A., Michielin, O. & Zoete, V. SwissTargetPrediction: updated data and new features for efficient prediction of protein targets of small molecules. *Nucleic Acids Res.* **47**, W357–W364. https://doi.org/10.1093/nar/gkz382 (2019).

36. Tacutu, R. et al. Human ageing genomic resources: new and updated databases. *Nucleic Acids Res.* **46**, D1083-D1090. https://doi.org/10.1093/nar/gkx1042 (2018).
37. Kanehisa, M. & Goto, S. KEGG: kyoto encyclopedia of genes and genomes. *Nucleic Acids Res.* **28**, 27–30. https://doi.org/10.1093/nar/28.1.27 (2000).
38. Kanehisa, M. Toward understanding the origin and evolution of cellular organisms. *Protein Sci.* **28**, 1947–1951. https://doi.org/10.1002/pro.3715 (2019).
39. Kanehisa, M., Furumichi, M., Sato, Y., Kawashima, M. & Ishiguro-Watanabe, M. KEGG for taxonomy-based analysis of pathways and genomes. *Nucleic Acids Res.* **51**, D587–D592. https://doi.org/10.1093/nar/gkac963 (2023).
40. Friedman, J., Hastie, T. & Tibshirani, R. Regularization paths for generalized linear models via coordinate descent. *J. Stat. Softw.* **33**, 1–22 (2010).
41. Furey, T. S. et al. Support vector machine classification and validation of cancer tissue samples using microarray expression data. *Bioinformatics* **16**, 906–914. https://doi.org/10.1093/bioinformatics/16.10.906 (2000).
42. Percie du Sert. Reporting animal research: explanation and elaboration for the ARRIVE guidelines 2.0. *PLoS Biol.* **18**, e3000411. https://doi.org/10.1371/journal.pbio.3000411 (2020).
43. Zhong, J. et al. Clock knockdown attenuated reactive oxygen species-mediated senescence of chondrocytes through restoring autophagic flux. *Life Sci.* **269**, 119036. https://doi.org/10.1016/j.lfs.2021.119036 (2021).
44. Feng, C. et al. ROS: crucial intermediators in the pathogenesis of intervertebral disc degeneration. *Oxid. Med. Cell. Longev.* **2017** (5601593). https://doi.org/10.1155/2017/5601593 (2017).
45. Bolduc, J. A., Collins, J. A. & Loeser, R. F. Reactive oxygen species, aging and articular cartilage homeostasis. *Free Radic. Biol. Med.* **132**, 73–82. https://doi.org/10.1016/j.freeradbiomed.2018.08.038 (2019).
46. Yu, L., Hao, Y., Xu, C., Zhu, G. & Cai, Y. LINC00969 promotes the degeneration of intervertebral disk by sponging mir-335-3p and regulating NLRP3 inflammasome activation. *IUBMB Life.* **71**, 611–618. https://doi.org/10.1002/iub.1989 (2019).
47. Penolazzi, L. et al. MicroRNA-221 silencing attenuates the degenerated phenotype of intervertebral disc cells. *Aging (Albany NY)*. **10**, 2001–2015. https://doi.org/10.18632/aging.101525 (2018).
48. Song, J. et al. CircularRNA_104670 plays a critical role in intervertebral disc degeneration by functioning as a ceRNA. *Exp. Mol. Med.* **50**, 1–12. https://doi.org/10.1038/s12276-018-0125-y (2018).
49. Feng, C. et al. Disc cell senescence in intervertebral disc degeneration: causes and molecular pathways. *Cell. Cycle.* **15**, 1674–1684. https://doi.org/10.1080/15384101.2016.1152433 (2016).
50. Cao, S. et al. An oxidative stress-related gene pair (CCNB1/PKD1), competitive endogenous RNAs, and Immune-infiltration patterns potentially regulate intervertebral disc Degeneration Development. *Front. Immunol.* **12**, 765382. https://doi.org/10.3389/fimmu.2021.765382 (2021).
51. Xu, S., Fu, H., Weng, S., Gu, X. & Li, J. Derivation and comprehensive analysis of ageing-related genes in intervertebral disc degeneration for prediction and immunology. *Mech. Ageing Dev.* **211**, 111794. https://doi.org/10.1016/j.mad.2023.111794 (2023).
52. Khan, A. N. et al. Inflammatory biomarkers of low back pain and disc degeneration: a review. *Ann. N Y Acad. Sci.* **1410**, 68–84. https://doi.org/10.1111/nyas.13551 (2017).
53. Karamouzian, S. et al. Effect of atorvastatin on angiogenesis in degenerated intervertebral disc in rat. *Spine (Phila Pa. 1976)*. **36**, 1824–1828. https://doi.org/10.1097/BRS.0b013e3181d4e15a (2011).
54. Zeldin, L. et al. Spatial mapping of collagen content and structure in human intervertebral disk degeneration. *JOR Spine*. **3**, e1129. https://doi.org/10.1002/jsp2.1129 (2020).
55. Ganko, R., Rao, P. J., Phan, K. & Mobbs, R. J. Can bacterial infection by low virulent organisms be a plausible cause for symptomatic disc degeneration? A systematic review. *Spine (Phila Pa. 1976)*. **40**, E587–592. https://doi.org/10.1097/BRS.0000000000000832 (2015).
56. Lan, W., Wang, X., Tu, X., Hu, X. & Lu, H. Different phylotypes of Cutibacterium acnes cause different modic changes in intervertebral disc degeneration. *PLoS One*. **17**, e0270982. https://doi.org/10.1371/journal.pone.0270982 (2022).
57. Schweizer, T. A. et al. Intervertebral disc cell chondroptosis elicits neutrophil response in Staphylococcus aureus Spondylodiscitis. *Front. Immunol.* **13**, 908211. https://doi.org/10.3389/fimmu.2022.908211 (2022).
58. Zhou, C. et al. Morroniside attenuates nucleus pulposus cell senescence to alleviate intervertebral disc degeneration via inhibiting ROS-Hippo-p53 pathway. *Front. Pharmacol.* **13**, 942435. https://doi.org/10.3389/fphar.2022.942435 (2022).
59. Risbud, M. V. & Shapiro, I. M. Role of cytokines in intervertebral disc degeneration: pain and disc content. *Nat. Rev. Rheumatol.* **10**, 44–56. https://doi.org/10.1038/nrrheum.2013.160 (2014).
60. Dinarello, C. A. Interleukin-1 in the pathogenesis and treatment of inflammatory diseases. *Blood* **117**, 3720–3732. https://doi.org/10.1182/blood-2010-07-273417 (2011).
61. Fang, W. et al. Wogonin mitigates intervertebral disc degeneration through the Nrf2/ARE and MAPK signaling pathways. *Int. Immunopharmacol.* **65**, 539–549. https://doi.org/10.1016/j.intimp.2018.10.024 (2018).
62. Li, X. et al. Resveratrol attenuates inflammation environment-induced nucleus pulposus cell senescence in vitro. *Biosci. Rep.* **39**. https://doi.org/10.1042/BSR20190126 (2019).
63. Chen, Z. B. et al. The role of quinazoline in ameliorating intervertebral disc degeneration by inhibiting oxidative stress and anti-inflammation via NF-kappaB/MAPKs signaling pathway. *Eur. Rev. Med. Pharmacol. Sci.* **24**, 2077–2086. https://doi.org/10.26355/eurrev_202002_20387 (2020).
64. Vassilieva, I. et al. Paracrine senescence of human endometrial mesenchymal stem cells: a role for the insulin-like growth factor binding protein 3. *Aging (Albany NY)*. **12**, 1987–2004. https://doi.org/10.18632/aging.102737 (2020).
65. Fang, P., Hwa, V., Little, B. M. & Rosenfeld, R. G. IGFBP-3 sensitizes prostate cancer cells to interferon-gamma-induced apoptosis. *Growth Horm. IGF Res.* **18**, 38–46. https://doi.org/10.1016/j.ghir.2007.07.002 (2008).
66. Lee, H. Y. et al. Insulin-like growth factor binding protein-3 inhibits the growth of non-small cell lung cancer. *Cancer Res.* **62**, 3530–3537 (2002).
67. Ushakov, R. E. et al. Chondrogenic differentiation followed IGFBP3 loss in human endometrial mesenchymal stem cells. *Biochem. Biophys. Res. Commun.* **531**, 133–139. https://doi.org/10.1016/j.bbrc.2020.07.064 (2020).
68. Wang, J. et al. Vascular smooth muscle cell senescence promotes atherosclerosis and features of Plaque vulnerability. *Circulation* **132**, 1909–1919. https://doi.org/10.1161/CIRCULATIONAHA.115.016457 (2015).
69. Baar, M. P., Perdiguero, E., Munoz-Canoves, P. & de Keizer, P. L. Musculoskeletal senescence: a moving target ready to be eliminated. *Curr. Opin. Pharmacol.* **40**, 147–155. https://doi.org/10.1016/j.coph.2018.05.007 (2018).
70. Lee, S. & Schmitt, C. A. The dynamic nature of senescence in cancer. *Nat. Cell. Biol.* **21**, 94–101. https://doi.org/10.1038/s41556-018-0249-2 (2019).
71. Zhang, P. et al. Senolytic therapy alleviates Abeta-associated oligodendrocyte progenitor cell senescence and cognitive deficits in an Alzheimer's disease model. *Nat. Neurosci.* **22**, 719–728. https://doi.org/10.1038/s41593-019-0372-9 (2019).
72. Wang, F., Cai, F., Shi, R., Wang, X. H. & Wu, X. T. Aging and age related stresses: a senescence mechanism of intervertebral disc degeneration. *Osteoarthr. Cartil.* **24**, 398–408. https://doi.org/10.1016/j.joca.2015.09.019 (2016).
73. Zhao, C. Q. et al. ADAMTS-5 and intervertebral disc degeneration: the results of tissue immunohistochemistry and in vitro cell culture. *J. Orthop. Res.* **29**, 718–725. https://doi.org/10.1002/jor.21285 (2011).
74. Bedore, J., Leask, A. & Seguin, C. A. Targeting the extracellular matrix: matricellular proteins regulate cell-extracellular matrix communication within distinct niches of the intervertebral disc. *Matrix Biol.* **37**, 124–130. https://doi.org/10.1016/j.matbio.2014.05.005 (2014).

75. Yeh, C. H. et al. Hesperetin promotes longevity and delays aging via activation of Cisd2 in naturally aged mice. *J. Biomed. Sci.* **29**, 53. https://doi.org/10.1186/s12929-022-00838-7 (2022).

76. An, Y. et al. Oridonin delays aging through the AKT signaling pathway. *Front. Pharmacol.* **13**, 888247. https://doi.org/10.3389/fphar.2022.888247 (2022).

Author contributions

T.X.K., Z.J.L., and L.H. conducted the literature review and data analysis and produced the manuscript. The majority of experiments and data analysis were carried out by T.X.K., Z.J.L., and L.H. Project design and article composition were collaboratively performed by T.X.K., Z.J.L., and L.H. Figure and spelling were validated by Z.F.X., W.L.X., L.S.J. X.J.C., L.H. and Z.Z.H. subsequently revised the manuscript. C.K. and Y.H.G. oversaw all aspects of manuscript design, supervision, and revision. All authors reviewed and assented to the final version of the manuscript.

Funding

Declarations

Competing interests

The authors declare no competing interests.

Ethics statement

The animal studies involved in this study were approved by the Ethics Committee of the First Affiliated Hospital of Nanchang University.

Additional information

Correspondence and requests for materials should be addressed to H.Y. or K.C.

Reprints and permissions information is available at www.nature.com/reprints.

Publisher's note Springer Nature remains neutral with regard to jurisdictional claims in published maps and institutional affiliations.